Acta Polytechnica CTU Proceedings **54**:72–78, 2025
https://doi.org/10.14311/APP.2025.54.0072

Published by the Czech Technical University in Prague

CHARACTERIZATION OF THE MICROSTRUCTURE OF CEMENT PASTE EXPOSED TO GAMMA RADIATION BY SCANNING ELECTRON MICROSCOPY

Andrea Špaková[a], Jiří Němeček[1,a,*], Lukáš Procházka[b], Patricie Halodová[b], Jiří Němeček[2,a]

[a] *Czech Technical University in Prague, Faculty of Civil Engineering, Department of Mechanics, Thákurova 7, 166 29 Prague 6, Czech Republic*

[b] *Research Centre Řež, Hlavní 130 Řež, Husinec 250 68, Czech Republic*

[*] corresponding author: jiri.nemecek.1@fsv.cvut.cz

Abstract. Hardened cement paste with a water-cement ratio of 0.4 was examined under five different relative humidity (RH) conditions (11 %, 33 %, 76 %, 96 %, and 100 %). These samples were exposed to gamma radiation with a total dose of 13.82 MGy over 341 days. Scanning electron microscopy (SEM) was the primary tool used for characterizing the samples' microstructure at a microscale, aided by image analysis (IA), which showed negligible changes in Calcium-Silicate-Hydrate phases but a decrease in Portlandite of 1.5–3.5 % under 33–100 % RH conditions. Point elemental analysis was conducted to determine the (Ca-S)/Si ratio of the inner product, finding a significant increase of up to 20 % at medium RH conditions (33–76 %).

Keywords: Electron microscopy, cement paste, gamma radiation.

1. Introduction

Concrete is a widely used construction material, essential for many different applications, including radiation shielding in light water reactors. These shields protect the power-plants by absorbing and dissipating the harmful irradiation caused by neutron fluxes and gamma-rays emitted from the reactor pressure vessel (RPV). Typical concrete members exposed to irradiation are the RPV pedestal and primary shielding wall of a boiling water reactor (BWR), and those of a pressurized water reactor (PWR), as shown in Figure 1 [1–3].

Currently, more than half of the existing nuclear reactors, including RPVs, are aging and reaching their design lifetimes of 40–60 years, presenting two primary options: shutting down or extending their operating licenses. The approximate lifetime extension is typically 20 years and in many cases, prolonging the current function is preferred over closing operations. This approach eliminates the need to build new power-plant reactors while the old ones still generate the required power. To facilitate the extension safely, it is crucial to closely investigate the impact of gamma and neutron radiation on concrete structures, aiming to find solutions for prolonging the functionality of power-plants worldwide by repairing, maintaining, or replacing the existing structures [1, 3, 4].

The projected doses on concrete after the designed lifetime of 80 years of power-plant operation are 100–200 MGy of gamma irradiation and approximately 6×10^{19} n cm^{-2} (E > 0.1 MeV) in neutron fluxes. This exposure leads to heat generation and progressive concrete degradation, resulting in a 20 % drop in compressive strength associated with deterioration of properties due to both internal and aggregate damage mechanisms [1, 5].

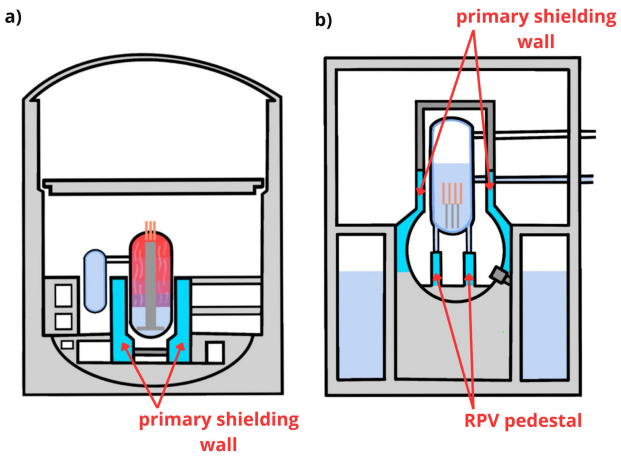

Figure 1. Typical concrete members subjected to irradiation in a) BWR, b) PWR [2].

Neutrons (E > 10–100 keV) cause radiation-induced volumetric expansion (RIVE) through metamictization (amorfization) of minerals in aggregates present in concrete. This process creates lattice structure defects, such as vacancies or interstitials, leading to significant changes in the volume and density of the minerals, which alters properties of concrete, includ-

[1] Postdoctoral researcher at Czech Technical University in Prague, Orcid: 0000-0002-5635-695X.

[2] Professor at Czech Technical University in Prague, Orcid: 0000-0002-3565-8182.

Cement	CaO	SiO_2	Al_2O_3	Fe_2O_3	MgO	Na_2O	K_2O	SO_3	Cl^-	MnO
CEM I 42.5 R (wt. %)	64.78	20.28	4.87	3.55	1.34	0.14	0.76	3.04	0.028	–

TABLE 1. Percentage representation of CEM I 42.5 R components (XRF data provided by manufacturer).

ing tensile strength, compressing strength, and elastic modulus [2].

Gamma rays can significantly affect concrete, in particular the Calcium-Silicate-Hydrate (C-S-H) gel, through dehydration caused by water radiolysis. Water radiolysis is a chemical reaction in which the interstitial liquid of C-S-H gel down chemical bonds, resulting in the formation and accumulation of explosive gases such as hydrogen (H_2). During this process, hydrogen gas (H_2), and other stable molecules (H_2O_2, H^+, OH^-), as well as highly unstable radicals ($H^{\cdot}$, $OH^{\cdot}$, e^-_{aq}), are formed. Hydrogen peroxide (H_2O_2) then reacts with CH and AFt, forming other unstable products, and by further reactions of those, $CaCO_3$ creation is obtained [4, 6].

Based on the testing of gamma-irradiated cementitious samples, the following observations were made [3]:

- The formation of the vaterite and aragonite, rather than calcite, occurs during carbonation. Vaterite formation in cement pastes was found to fill pores around the C-S-H gel, resulting in increased stiffness and bending strength [4].
- It has been shown, that evaporable water decomposes readily under gamma-ray irradiation in cement pastes and over a long-period exposure of a high dosage of gamma-rays was found, that in 1 % can be decomposed even chemically bound water [7].
- Irradiation of C-S-H pellets at a dosage of 189 MGy and 11 % relative humidity (RH) resulted in a decrease in the basal spacing of the C-S-H gel by 0.5–0.7 Å. This decrease is associated with a reduction in molecular water content and an increase in hydroxyl groups in the C-S-H gel. Nanoindentation, performed with a maximum force of 4 mN, revealed a 15–25 % increase in Young's modulus in irradiated samples [1].
- Nanoindentation of samples irradiated at below 11 % RH showed an approximately 25 % increase in nanoindentation Young's modulus due to a combination of water radiolysis and drying, resulting in the densification of the C-S-H gel at a nanoscale level of 100 nm. This densification was accompanied by microcracking, which caused a decrease in the microindentation Young's modulus by ∼17 % at the higher scale of 20 µm [8].
- Samples irradiated under common RH conditions (30–60 %) showed minimal differences in nanomechanical properties measured by nanoindentation of cement paste [8] and mortar [9].
- The samples irradiated in water, representing 100 % RH, a significant decrease in nanoindentation Young's modulus by 26 % of the main hydrates, along with a simultaneous loss of Portlandite by 9–10 %, was observed [8].
- Ordinary cement paste samples exposed to gamma doses of 0–1188 MGy were analyzed using scanning electron microscopy (SEM) and X-ray diffraction (XRD). Starting at a dose of 130 MGy, a decrease in crystalline phases formed during hydration was observed by XRD, and with increasing dosage, this decrease became more pronounced, accompanied by clinker decomposition. The development of pseudomorphoses, along with the formation of bubbles and cracks due to the separation of chemically bound water, was also observed by SEM at a dose of 290 MGy [10].

Since gamma radiation can significantly alter the mechanical and chemical properties of cementitious composites, depending on the RH conditions during irradiation. This paper focuses on the characterization of the chemical composition of ordinary cement paste exposed to five different RH conditions using scanning electron microscopy. The results presented in this paper were also reported in the author's bachelor's thesis [3].

2. Experiments and methods

2.1. Sample preparation

A cement paste mixture with a water-cement ratio of 0.4 was prepared using Portland cement CEM I 42.5 R. The percentage representation of components in the Portland cement is shown in Table 1.

The mixture was poured into cylindrical plastic molds with a 27 mm diameter and 70 mm height and then vibrated. The samples were stored for 24 hours before being demolded. The solidified samples were stored in a 1 % lime water solution for 610 days (1.67 years). Afterward, the samples were extracted from the lime water and sliced to a height of approximately 19 mm using a diamond blade (Struers Secotom-50). The cut samples were then stored at five RH levels (11 %, 33 %, 76 %, 96 %, and 100 %). Four samples were kept in containers with salt solutions, while the fifth was submerged in water, representing 100 % RH. The salt solutions did not come in contact with the tested samples. A summary of specific salts and corresponding RH levels is provided in Table 2 [3].

RH (%)	11	33	76	96	100
Saturated salt	LiCl	$MgCl_2$	NaCl	KNO_3	–
Other condition	–	–	–	–	Water

Table 2. Summary of conditions controlling relative humidity.

2.2. Gamma irradiation

The samples in containers were left to stabilize at their respective RH conditions for 14 days. Half of the samples were then irradiated with Co^{60} for 341 days in the Research Centrum Řež, receiving a total dosage of 13.82 MGy and an average dose rate of 0.675–1.890 kGy/h. The second half of the control samples were kept under the same conditions but were not exposed to gamma radiation [11]. The labeling of the samples was XX–YY, where XX represents the specific RH condition (11/33/76/96/100), and YY denotes whether the sample was irradiated (Ir) or control (C) [3].

2.3. Sample preparation before electron microscopy

The surfaces of the samples were polished using a Struers Tegramin 20 machine. The required unscratched and evenly polished surfaces were achieved by applying various SiC foils with different grit sizes at varying speeds and pressure forces. The samples were polished without any lubricant while constantly sweeping free particles [3].

The polishing process began with a coarser # 1200 SiC foil, followed by # 2000, and finally # 4000. The samples were polished with # 4000 twice to avoid any damage from the accumulation of free particles on the sample. All foils used, along with the applied forces, rotation speeds, and total polishing times for each step, are listed in Table 3 [3].

After each step, the samples were placed in a flask filled with isopropyl alcohol and then into an ultrasonic cleaner (USC) for 1 minute to remove any free particles that could scratch the sample during subsequent polishing steps. After each USC process, the samples were dried with compressed air and prepared for the next procedure [3].

2.4. Scanning electron microscopy

A Phenom XL desktop SEM was used to characterize the phase composition of the cement paste samples. SEM provides high-resolution images that enable the distinction of different phases in cement pastes. In ordinary cement paste, five main phases are typically easy to recognize with SEM: inner and outer hydration products, Portlandite, residual clinker, and pores or cracks [3, 12, 13].

2.4.1. BSE imaging and image analysis

SEM-BSE (back-scattered electrons) images at 900× magnification, with a size of $298 \times 298\,\mu m^2$ and a pixel resolution of 146 nm, were captured for image analysis [3].

Data	Step 1	Step 2	Step 3
Foil roughness (–)	# 1200	# 2000	# 4000
Disk rpm (–)	100	120	120
Head rpm (–)	70	70	70
Time (s)	10	60	150
Force (N)	10	10	5

Table 3. Summary of polishing steps with corresponding rotation speed (rpm), duration, applied force, and SiC foil roughness.

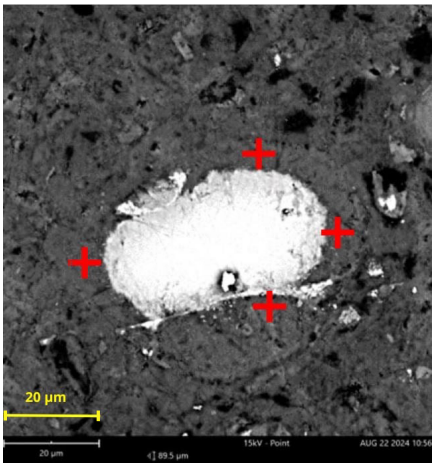

Figure 2. Selected image points (red crosses) around the residual clinker were used in EDS Point Analysis in the inner product of the 100–Ir sample.

The accelerating voltage was set to 15 kV. A total of ten images were taken for each sample, covering a total area of 0.888 mm^2. Each of these images was in 8-bit format with grayscale pixel values ranging from 0 to 255 [3].

2.4.2. Point element analysis

Energy Dispersive X-ray Spectroscopy (EDS) was used to analyze the chemical composition of the inner product formed around residual clinker grains, in point mode, at 3000× magnification. The images had a size of $89.5 \times 89.5\,\mu m^2$. A BSD full detector and an accelerating voltage of 15 kV were used. In total, twenty different points in inner product around at least seven clinker grains were analyzed for each sample, as shown in Figure 2. Only the inner product phase was selected since phase mixture is less frequent in this phase contrary to outer product [12].

3. Results and discussion

A typical SEM-BSE image for irradiated and control samples at 33 % RH is shown in Figure 3. Five distinct phases were identified: residual clinker, Portlandite, inner product, outer product, and cracks and pores. However, due to the overlapping grayscale threshold between the inner and outer product phases [13],

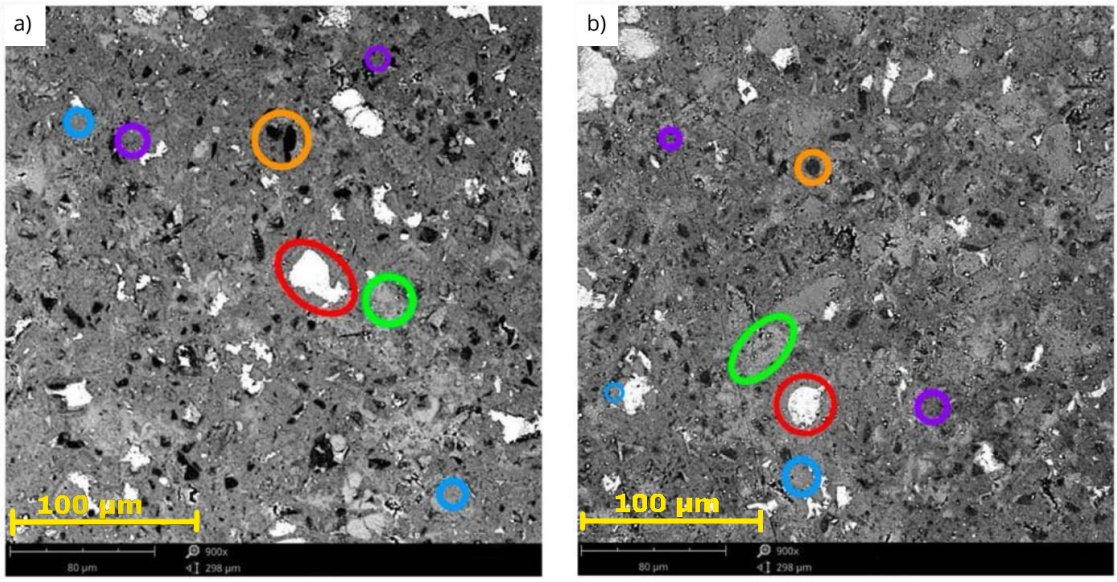

FIGURE 3. SEM-BSE images of samples a) 33–Ir, b) 33–C, highlighting five main phases: orange – pores and scratches, red – residual clinker, green – Portlandite, cyan – inner product, purple – outer product.

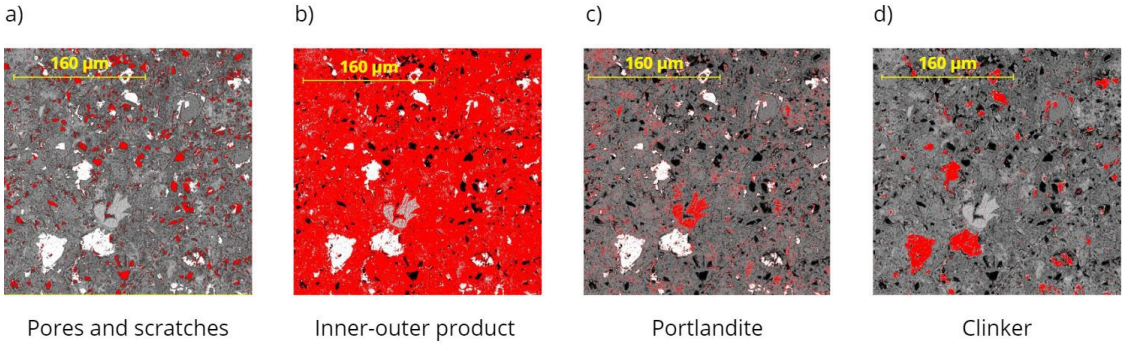

FIGURE 4. Example of phase separation for the 100–Ir sample using image analysis for individual phases: a) pores and scratches, b) inner-outer product, c) Portlandite, d) clinker.

these phases were grouped together and referred to as the "inner-outer product" during image analysis. An example of this separation process is illustrated for the 100–Ir sample in Figure 4. The grayscale threshold boundaries for this image were estimated as follows: residual clinker (255 to 185), Portlandite (184 to 150), inner-outer product (149 to 41), and pores and scratches (40 to 0) [11]. The mean values and standard deviations for each irradiated and control sample are summarized in Figure 5.

The results of image analysis show minimal changes between irradiated and control samples across all RH levels. Almost negligible changes are observed in the inner-outer product phase. Samples at 100 % RH show a slight decrease in residual clinker by ≈1 % and in the pores/cracks phase by ≈2 % compared to samples stored at other RH conditions. This suggests that these changes were primarily due to continuous hydration, not irradiation. A slight decrease in Portlandite by 1.5–3.5 % was observed at 33 %, 76 %, 96 %, and 100 % RHs, suggesting decomposition due to irradiation, which is in accordance with other studies [8, 10]. However, the measured changes are within the accuracy of the method, and for a more precise estimation of Portlandite, thermogravimetric measurements will be performed in the future.

Additionally, SEM-BSE images were examined for crack formation due to gamma radiation. In this case, no cracks were observed in either the irradiated or control samples. This finding does not align with other studies. However, in the study by Łowi'nska-Kluge and Piszora [10], crack formation was observed after a gamma dose of 130 MGy, which is ten times higher than the dose used in our study. In the study by Němeček et al. [8], crack formation in irradiated samples was only pronounced after prolonged exposure to the SEM vacuum chamber [11].

Point EDS analysis was performed in the inner product phase formed around clinker grains, as marked in Figure 2. The typical elemental spectrum of this spot is shown in Figure 6 for the 100–Ir sample. The elemental atomic concentrations and the stoichiomet-

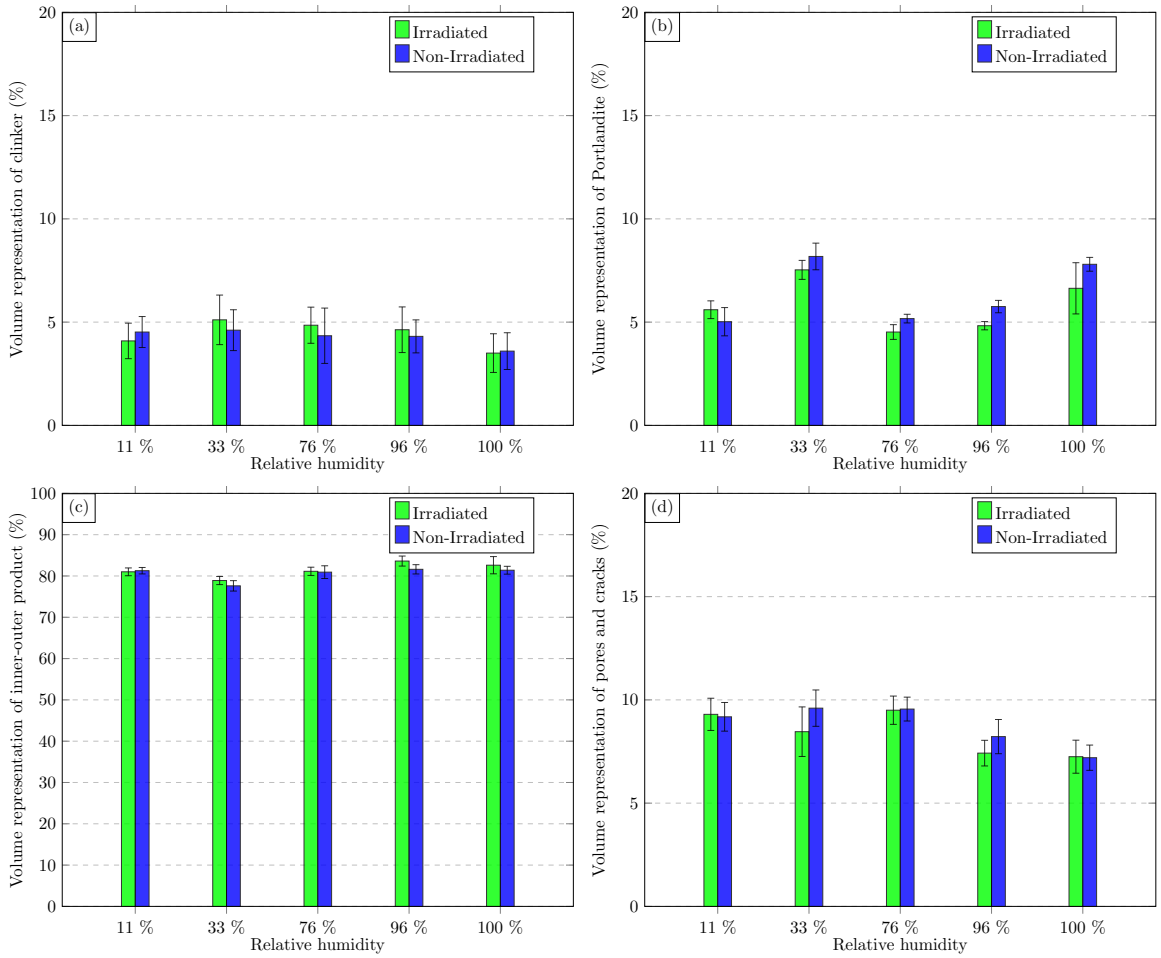

Figure 5. Image analysis results of (a) clinker, (b) Portlandite, (c) inner-outer product, (d) pores and cracks

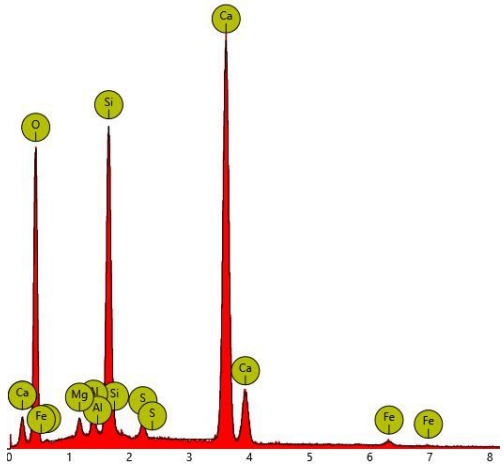

Figure 6. Typical SEM–EDS elemental spectrum of the inner product measured on the 100–Ir sample.

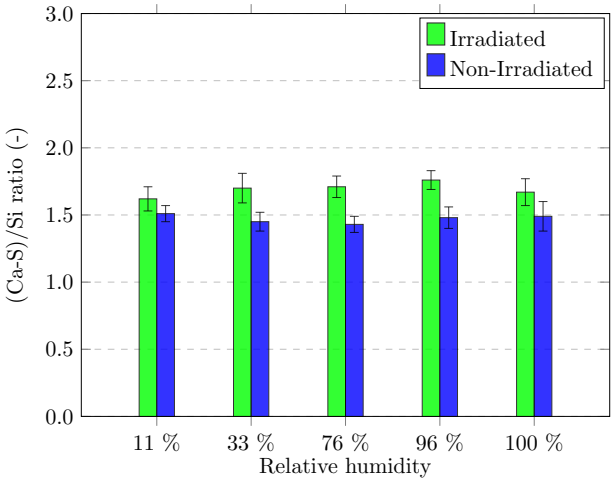

Figure 7. The mean value and standard deviation of the (Ca-S)/Si ratio measured by EDS Point Analysis.

ric weight concentrations of oxides for the 100–Ir and 100–C samples are presented in Table 4. Additionally, the (Ca-S)/Si ratios were calculated for all samples and are shown and compared with each other in Figure 7.

Results of the EDS point analysis indicated an increase in the (Ca-S)/Si ratio of irradiated samples. A smaller increase is observed at the lowest and highest RH conditions, specifically by 7.3 % at 11 % RH and 12.1 % at 100 % RH. However, a more significant increase in the (Ca-S)/Si ratio is noted for samples at middle RH levels, with increases of 18.1 % at 33 % RH, 19.6 % at 76 % RH, and 18.9 % at 96 % RH. The

Element symbol	Atomic Conc. 100–Ir (%)	100–C (%)	Oxide symbol	Stoich. wt. Conc. 100–Ir (%)	100–C (%)
O	53.40	57.9	–	–	
Ca	30.81	27.33	CaO	57.11	55.88
Si	11.62	10.60	SiO_2	32.97	34.66
Mg	1.05	0.78	MgO	2.28	1.92
Al	1.06	1.33	Al_2O_3	2.67	3.66
Fe	1.33	1.04	Fe_2O_3	2.66	2.16
S	0.84	0.59	SO_3	2.53	2.10

TABLE 4. Percentage representation of elements and their oxides in the inner product around residual clinker, as determined using EDS Point Analysis at typical measured points.

minimal changes observed at 11 % RH are consistent with the negligible changes reported for synthetically gamma-irradiated C-S-H pellets at 11 % RH [1, 14]. This was accompanied by an increase in the nanoindentation Young's modulus [1], which is also characteristic of cement paste samples [8].

4. Conclusions

This study investigated gamma-irradiated ordinary cement paste (total dose of 13.82 MGy) exposed to five different RH levels (11–100 %) using scanning electron microscopy. Based on the observation of BSE images and EDS point analysis, the following conclusions were drawn:

- A negligible change in C-S-H gel volume fraction between irradiated and control samples was observed across all RH levels.
- At a dosage of 13.82 MGy, a 1.5–3.5 % decrease in the Portlandite phase was observed for RH conditions ranging from 33–100 %, indicating degradation due to gamma irradiation.
- Observation of SEM-BSE images showed no visible crack formation in either the irradiated or control samples across all RH levels.
- A significant increase in the (Ca-S)/Si ratio of the inner product was observed for samples irradiated at medium RH, specifically 18.1 % at 33 % RH and 19.6 % at 76 % RH.

Acknowledgements

This work was financially supported by the Czech Science Foundation grant project 23-05435S and the Grant Agency of the Czech Technical University in Prague (SGS25/083/OHK1/2T/11). The presented results were obtained using the CICRR infrastructure, which is financially supported by the Ministry of Education and Culture – project LM2023041.

References

[1] A. Baral, E. T. Rodriguez, W. A. Hunnicutt, et al. Ultra-high gamma irradiation of calcium silicate hydrates: Impact on mechanical properties, nanostructure, and atomic environments. *Cement and Concrete Research* **158**:106855, 2022. https://doi.org/10.1016/j.cemconres.2022.106855

[2] I. Maruyama, O. Kontani, M. Takizawa, et al. Development of soundness assessment procedure for concrete members affected by neutron and gamma-ray irradiation. *Journal of Advanced Concrete Technology* **15**(9):440–523, 2017. https://doi.org/10.3151/jact.15.440

[3] A. Špaková. *Effect of gamma radiation and relative humidity on cement pastes microstructure studied by scanning electron microscopy.* Bachelor thesis, Czech technical university in Prague, 2025.

[4] I. Maruyama, S. Ishikawa, J. Yasukouchi, et al. Impact of gamma-ray irradiation on hardened white Portland cement pastes exposed to atmosphere. *Cement and Concrete Research* **108**:59–71, 2018. https://doi.org/10.1016/j.cemconres.2018.03.005

[5] K. Field, I. Remec, Y. L. Pape. Radiation effects in concrete for nuclear power plants – Part I: Quantification of radiation exposure and radiation effects. *Nuclear Engineering and Design* **282**:126–143, 2015. https://doi.org/10.1016/j.nucengdes.2014.10.003

[6] P. Bouniol, A. Aspart. Disappearance of oxygen in concrete under irradiation: the role of peroxides in radiolysis. *Cement and Concrete Research* **28**(11):1669–1681, 1998. https://doi.org/10.1016/S0008-8846(98)00138-0

[7] O. Kontani, S. Sawada, I. Maruyama, et al. Evaluation of irradiation effects on concrete structure: Gamma-ray irradiation tests on cement paste. In *ASME Power Conference*, vol. 56062. American Society of Mechanical Engineers, 2013. V002T07A002.

[8] J. Němeček, P. Trávníček, M. Keppert, et al. Nanomechanical analysis of Gamma-irradiated cement paste exposed to different humidities. *Construction and Building Materials* **393**:131969, 2023. https://doi.org/10.1016/j.conbuildmat.2023.131969

[9] Y. Khmurovska, P. Štemberk, S. Sikorin, et al. Effects of gamma-ray irradiation on hardened cement mortar. *International Journal of Concrete Structures and Materials* **15**(1):17, 2021. https://doi.org/10.1186/s40069-020-00452-7

[10] A. Łowińska-Kluge, P. Piszora. Effect of gamma irradiation on cement composites observed with XRD and SEM methods in the range of radiation dose 0-1409 MGy. *Acta Physica Polonica A* **114**(2):399–411, 2008. https://doi.org/10.12693/APhysPolA.114.399

[11] J. Němeček, A. Špaková, J. Němeček, P. Halodová. Micro-scale properties of cement pastes exposed to gamma radiation. *Acta Polytechnica CTU Proceedings* **53**:76–81, 2025. https://doi.org/10.14311/APP.2025.53.0076

[12] K. L. Scrivener. Backscattered electron imaging of cementitious microstructures: understanding and quantification. *Cement and Concrete Composites* **26**(8):935–945, 2004. Scanning electron microscopy of cements and concretes. https://doi.org/10.1016/j.cemconcomp.2004.02.029

[13] J. Němeček, J. Lukeš, J. Němeček. High-speed mechanical mapping of blended cement pastes and its comparison with standard modes of nanoindentation. *Materials Today Communications* **23**:100806, 2020. https://doi.org/10.1016/j.mtcomm.2019.100806

[14] E. E. T. Rodriguez, W. A. Hunnicutt, P. Mondal, Y. Le Pape. Examination of gamma-irradiated calcium silicate hydrates. Part I: Chemical-structural properties. *Journal of the American Ceramic Society* **103**(1):558–568, 2020. https://doi.org/10.1111/jace.16515